ACS MEASUREMENT SCIENCE Au
AN OPEN ACCESS JOURNAL OF THE AMERICAN CHEMICAL SOCIETY

pubs.acs.org/measureau

Article

Electrochemical Capillary Driven Immunoassay for Detection of SARS-CoV-2

Kaylee M. Clark,[†] Melissa S. Schenkel,[†] Trey W. Pittman, Isabelle C. Samper, Loran B. R. Anderson, Wisarut Khamcharoen, Suad Elmegerhi, Rushika Perera, Weena Siangproh, Alan J. Kennan, Brian J. Geiss, David S. Dandy, and Charles S. Henry*

Cite This: *ACS Meas. Sci. Au* 2022, 2, 584–594

Read Online

ACCESS | Metrics & More | Article Recommendations | Supporting Information

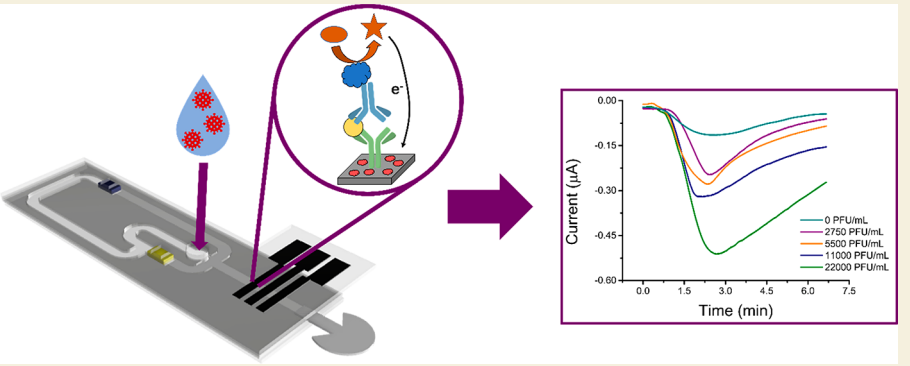

ABSTRACT: The COVID-19 pandemic focused attention on a pressing need for fast, accurate, and low-cost diagnostic tests. This work presents an electrochemical capillary driven immunoassay (eCaDI) developed to detect SARS-CoV-2 nucleocapsid (N) protein. The low-cost flow device is made of polyethylene terephthalate (PET) and adhesive films. Upon addition of a sample, reagents and washes are sequentially delivered to an integrated screen-printed carbon electrode for detection, thus automating a full sandwich immunoassay with a single end-user step. The modified electrodes are sensitive and selective for SARS-CoV-2 N protein and stable for over 7 weeks. The eCaDI was tested with influenza A and Sindbis virus and proved to be selective. The eCaDI was also successfully applied to detect nine different SARS-CoV-2 variants, including Omicron.

KEYWORDS: *SARS-CoV-2, immunoassay, biosensor, electrochemistry, screen-printed carbon electrodes, fluidic device*

INTRODUCTION

The outbreak of COVID-19, caused by the infectious severe acute respiratory syndrome coronavirus-2 (SARS-CoV-2), shed light on the need for developments in effective point-of-care diagnostics.[1] To date, a large number of COVID-19 tests have been approved by the U.S. Food and Drug Administration[2] and even more published in academic literature.[3−5] Despite the options available for point-of-care testing, the recommended and most sensitive testing option is reverse transcriptase polymerase chain reaction (rt-PCR). Rt-PCR tests detect the viral RNA and remain the gold standard for testing, as they have the lowest limits of detection (LODs) and highest specificity.[6] Unfortunately, the rt-PCR assay takes hours to complete, so depending on the site of sample collection it can take several days for a patient to receive a result.[7] Enzyme linked immunosorbent assays (ELISAs) are another diagnostic tool that can be used to detect COVID-19-associated antigens or antibodies.[7] Unfortunately, traditional ELISAs still need to be performed in a laboratory setting, require many tedious steps or complicated robotics, and can take several hours to complete.[8]

Alternatively, lateral flow assays (LFAs) have been developed to decrease the time to result and allow for diagnosis at the point-of-care.[9] These tests detect antigens or antibodies as opposed to viral RNA. Generally, the addition of a sample induces capillary flow through a nitrocellulose strip, and reagents dried within the device are delivered sequentially to the test and control lines, producing a colorimetric signal of two lines for a positive sample and one line for a negative sample. Unfortunately, these devices are rightfully criticized for their lack of sensitivity and limits of detection, especially compared to more sophisticated techniques like ELISA.[10,11]

Received: June 16, 2022
Revised: August 9, 2022
Accepted: August 16, 2022
Published: August 30, 2022

https://doi.org/10.1021/acsmeasuresciau.2c00037
ACS Meas. Sci. Au 2022, 2, 584–594

Microfluidic and other flow devices have been developed to perform traditional lab-based techniques like rt-PCR, rt-LAMP, nested PCR, nucleic acid hybridization, ELISA, and fluorescence based assays.[12] By reducing the sample volumes needed, these devices provide a platform that can control reactions, separations, delivery of reagents, and detections with high sensitivity, faster readouts, and a lower cost compared to the traditional techniques.[13] There have been many attempts to automate multistep assays such as ELISA in inexpensive flow devices.[14] The flow of reagent delivery has been controlled by chemical barriers,[15,16] physical barriers,[17,18] hydrophobic barriers,[19] and complex geometric fluid paths in the paper-based devices.[20,21] Many still require more than one user step.[19] In 2013, Apilux et al. introduced an automated sandwich ELISA with one sample addition step in a paper device.[20] This device was a promising step forward; however, paper devices have been known to suffer from slow and nonuniform flow and difficulties with particle and reagent transport..[22,23]

Capillary-driven fluidic devices have become popular due to their lack of need for external pumps and other laboratory equipment.[24] A new class of hollow channel capillary-driven devices using polyethylene terephthalate (PET) and double-sided adhesive (DSA) was recently introduced by our group, and these devices have been used to demonstrate advanced mixing and flow control[25,26] and applied to viscosity measurements[27] and SARS-CoV-2 serology tests.[28,29] While other examples of using PET for capillary-driven devices have been shown,[30] they lack the complexity necessary for sequential delivery and precise flow control.

Colorimetry is the most common detection mechanism for capillary-driven and paper-based flow devices, but it often suffers from low sensitivity and small linear ranges.[31] Electrochemical detection is an attractive alternative because it can be quick, cost-effective, accurate, highly sensitive, and quantitative.[32] Additionally, the double line readout of a traditional LFA relies on user interpretation and does not easily yield itself to quantitative detection. Further, there are many existing reports of improving LFA sensitivity by incorporating electrochemical transducers.[33] Electrodes have also been incorporated into various other flow devices to improve detection.[34,35] Additionally, electrodes have previously been used for e-ELISA, using electrochemistry as an alternate detection for traditional ELISA.[36−38]

Previous work presented a device for the detection of IgG antibodies against SARS-CoV-2 N proteins in whole blood;[29] however, this device required two distinct steps for the end user, making it difficult for untrained users to operate. While monitoring antibodies is useful to study immune response in an individual and the overall population, it cannot be used to detect active infection. To detect active infections, we sought to develop a modified system for direct detection of SARS-CoV-2 N protein. This work describes an electrochemical capillary driven immunoassay (eCaDI) device made from polyethylene terephthalate (PET) and adhesive films with an incorporated screen-printed carbon electrode system. Upon a one-step addition of a sample, the flow device sequentially delivers all the reagents necessary to perform an automated ELISA, producing quantitative detection of SARS-CoV-2.

METHODS

Reagents and Materials

Solutions were prepared using 18.2 MΩ·cm water purified using a Milli-Q system (MilliporeSigma, USA). Phosphate buffer saline (PBS) tablets, 3,3′,5,5′-tetramethylbenzidine (TMB), ethylenediaminetetraacetic acid (100%), ferrous sulfate heptahydrate (100%), sodium hydroxide (98.9%), D-(+)-trehalose dihydrate (100%), and sodium tetraborate (≥99%) were purchased from Sigma-Aldrich (Saint Louis, MO). Tween80 (pure), boric acid (99.5%), casein, 10× Stable Peroxide Buffer, bovine serum albumin (≥98%), and sucrose (≥99.5%) were purchased from Thermo Fisher Scientific (Waltham, MA). Commercial SARS-CoV-2 anti-N antibodies (MM08) and SARS-CoV-2 detection-HRP (MM05-H) antibodies were purchased from Sino Biological (Beijing, China). Igepal was purchased from MP Biomedicals (Irvine, CA). Unmodified glass fiber with PVA binder was purchased from MilliporeSigma (Burlington, MA). Zeba 40K Micro Spin Desalting Columns were purchased from Thermo Scientific (Rockford, IL). Polyethylene terephthalate sheets (2500 and 9984) and double-sided adhesive (467) were purchased from 3M (Saint Paul, MN). Carbon ink (CI-2057) was purchased from Engineered Materials Solutions, Inc. (Attleboro, MA). Dielectric ink was purchased from Dupont (Wilmington, DE).

Solutions

Phosphate buffer solution (PBS, 10 mM) with 140 mM sodium chloride and 2.7 mM potassium chloride, pH 7.4 was prepared by dissolving a tablet in DI water according to package instructions. Phosphate buffer solution (10 mM) with Tween20 (PBST) was made by adding 0.05% Tween20 to PBS. Antibody immobilization buffer was prepared by adding 0.0005% Tween 20 to PBS. Stable peroxide buffer (SPB) 1× was prepared by diluting commercial 10× stable peroxide buffer 1:10 and adding 0.1% Igepal and 0.1% Tween 80. Borate buffer, 1 M, pH 8.5, was prepared by dissolving boric acid in water and adding sodium hydroxide. The buffer was then diluted to 50 mM in water and used to dilute the aged casein blocker. A bulk solution of 6% aged casein was prepared as previously reported.[39] Briefly, 6 g of casein was dissolved in 80 mL of 50 mM sodium hydroxide overnight. Then 0.26 g boric acid and 0.45 g sodium tetraborate were added and the solution was pH adjusted to 8.5. The solution was diluted to 100 mL with Millipore distilled water and heated at 37 °C for 7 days. The aged casein was aliquoted and stored at −20 °C. Drying buffer was prepared as previously reported.[40] First, a 1 M solution of EDTA was prepared in PBS. Ferrous sulfate was added to a concentration of 0.01 M. Then 4% trehalose and 0.1% BSA was added, and the solution was stored at 4 °C for up to 3 months.

Inactivated Virus Samples

SARS-CoV-2 strains (USA-WA1/2020 = NR-52281, UK00 = NR-54000, UK11 = NR-54011, SA08 = NR-54008, SA09 = NR-54009, WA = NR-52281 (wildtype), Delta = NR-55486, Gamma = NR-54982, Kappa = NR-55486, Omicron = NR-56486) were obtained from BEI Resources and grown/quantified to produce viral stocks in BSL-3 containment in Vero E6 cells (ATCC (CRL-1586) in DMEM media containing 2% fetal bovine serum at 50 mM HEPES (pH 7.5). Stocks were stored at −80 °C in single-use aliquots. Viral stocks were quantified for infectivity via plaque assay (plaque-forming units (PFU)/ml) following procedures outlined in previous work.[41] Sindbis virus TE3′2J was quantified as described by Steel et al.,[42] and Influenza A (H1N1) A/Swine/1976/31 (ATCC VR-1682) virus was quantified on MDCK cells (ATCC CCL-34) essentially as previously described.[43] To inactivate all virus, viral stocks were thawed and 0.1% Igepal was added to a final concentration of 0.1% for 30 min on ice, followed by storage at −20 °C. All inactivated virus samples were verified for lack of infectivity prior to removal from BSL-2/BSL-3 containment via plaque assay. After the viruses were inactivated, all steps and experiments using inactivated virus were performed in a BSL-2 cabinet. Dilutions of inactivated viral stocks were made in stable peroxide buffer (SPB) immediately prior to addition to devices.

https://doi.org/10.1021/acsmeasuresciau.2c00037
ACS Meas. Sci. Au 2022, 2, 584−594

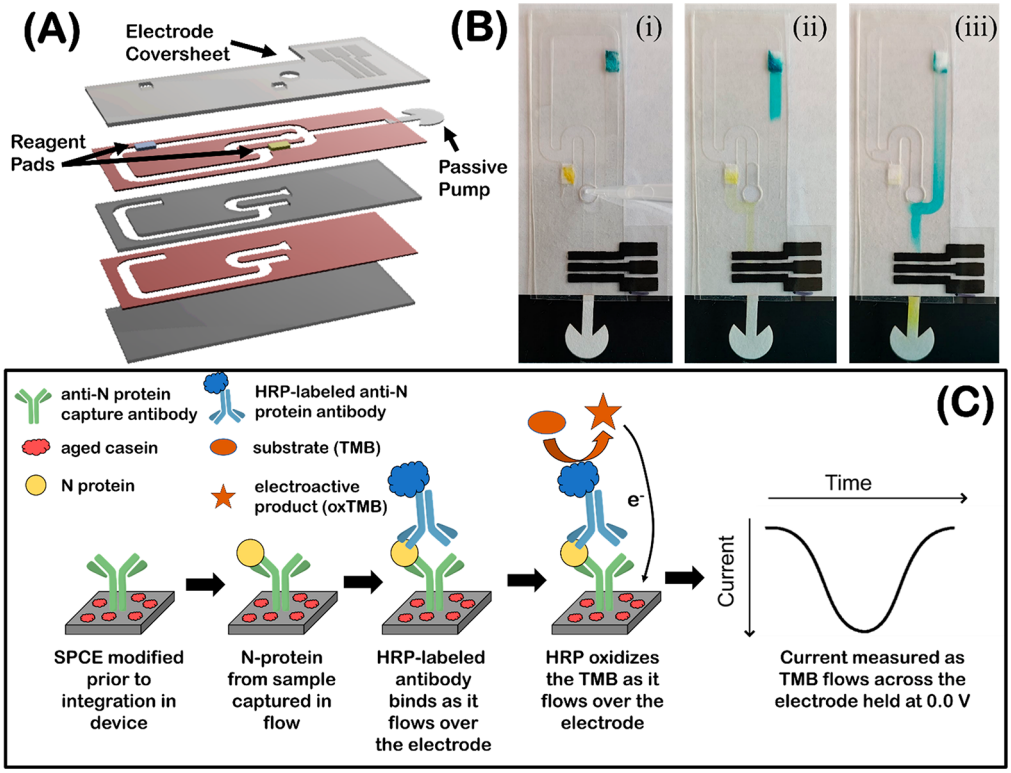

Figure 1. (A) Exploded view of eCaDI showing alternating PET (gray) and adhesive (red) layers. The second layer from the top shows the two reagent pads (blue = TMB, yellow = HRP ab) and the passive pump on the far right. (B) Flow of eCaDI: (i) addition of sample and sequential delivery of (ii) HRP-antibodies (with yellow dye) and (iii) TMB (with blue dye) to the SPCE. (C) Electrochemical immunoassay and detection mechanism, showing modified electrode, target capture, secondary antibody binding, turnover of substrate, and electrochemical detection.

Desalting and Quantification of Antibodies

MM08 and MM05-H antibodies were desalted using Zeba Spin Desalting Columns according to directions. Briefly, the columns were dried and then rinsed three times with PBS by spinning at 4700 rpm for 60 s. Then 7 μL of commercial antibody solution was added and the sample was spun for 2 min. MM08 was diluted 1:100 in antibody immobilization buffer and used immediately for electrode modification. MM05-H was diluted to 80 μL in PBS, quantified using variable path length UV/vis Solo-VPE (C Technologies, Inc., Bridgewater, NJ), diluted to 1 μg/mL in SPB for static experiments, and diluted to 20 μg/mL in drying buffer for fluidic experiments. More information on the quantification can be found in the Supporting Information (SI) (Figure SI1 and Table SI1).

Electrode Fabrication

A three-electrode system was screen printed on 3M 2500 PET film using carbon ink and a 305 count mesh screen. After printing, the ink was dried for 30 min at 60 °C. Dielectric ink wells were then screen-printed around the working electrode and UV cured until dry. The reference electrode was painted over with a thin layer of AglAgCl paste (Sigma-Aldrich Saint Louis, MO) and dried for 30 min at 60 °C. The electrode covers heets (PET sheets on which electrodes were screen printed) were then cut using a CO_2 laser cutter according to the device layout and serve as top layer of the device.

Electrode Modification with Drying Method

The electrodes were functionalized by drop-casting 10 μL of 10 μg/mL capture antibody (MM08) in antibody immobilization buffer onto the working electrode, inside the dielectric ink well. The electrodes were dried in a Petri dish at 37 °C for about 45 min. Once dry, 5 μL of 0.3% aged casein in 50 mM borate buffer was dropped into the dielectric well and allowed to dry at room temperature.

Device Fabrication

The fluidic devices were designed using CorelDRAW (Corel, Ontario, Canada) and cut using a CO_2 laser cutter (Zing 10000, Epilog Laser) to pattern layers of PET films (9984) and 3M 467 DSA and sandwich the layers together. Glass fiber conjugate release pads were cut to fit in a medium size Petri dish. A solution of 10 mM PBS was prepared with 0.1% thimersol and 0.5% Tween 20. Sucrose was added to a final concentration of 3% w/v. The glass fiber pad was fully submerged and soaked in this solution for 15 min at room temperature and then removed from the solution and dried in a 37 °C incubator overnight until completely dry. After pretreatment, pads were cut to 3 mm × 5 mm. TMB reagent pads were made by pipetting 5 μL of TMB solution onto pretreated glass fiber pads and incubated at 37 °C for 15 min. This process was repeated two additional times, resulting in 15 μL of TMB for each reagent pad. Next, 5 μL of 80× diluted Great Value blue food dye in Milli-Q distilled water was added and incubated at 37 °C for 1 h. The reason for adding food dye is to create a visual aid within the eCaDI that allows the operator to evaluate the flow through the device and determine the correct time to start the chronoamperometry measurement. HRP-antibody conjugate release pads were made by pipetting 5 μL of 20 μg/mL HRP conjugated secondary antibody solution onto glass fiber pads and incubated at 37 °C for 15 min. This process was repeated once, resulting in 10 μL of 20 μg/mL HRP-antibody solution for each reagent pad. Finally, 5 μL of 80× diluted Great Value yellow food dye in Milli-Q distilled water was added and incubated at 37 °C for 1 h. After preparation of both conjugate release pads, the pads were placed within the channels of the device, and the cover layer containing the functionalized electrode was placed on top and sealed to the exposed DSA. Devices were kept out of the light until used for experiments. Before use, a 17 mm diameter (shape shown in Figure 1) Whatman 1 chromatography paper waste pad was inserted to the opening at the bottom of the device.

https://doi.org/10.1021/acsmeasuresciau.2c00037
ACS Meas. Sci. Au 2022, 2, 584−594

Static Electrochemical Detection Method

For static assay experiments, wells made with 3M 467 double sided adhesive (DSA) mimicking the size of the fluidic channel were placed over the working, counter, and reference electrodes to confine the solutions. To complete the assay, 20 μL of inactivated virus, diluted in SPB, was dropped in the well and incubated for 30 min. After washing with PBST followed by PBS, 20 μL of 1 μg/mL labeled antibody (MM05-H) solution in SPB was dropped into the well and incubated for 25 min. The electrodes were washed a final time, and 20 μL of PBS was dropped until measurements could be taken. Just before the measurement, the 20 μL of PBS was removed with a pipet. Then 50 μL of TMB was added to the electrode surface, confined by the adhesive well, and incubated for 2 min. Immediately following the TMB incubation, a 2 min chronoamperometry measurement was started using a potentiostat (PalmSens4). A 0.0 V potential was applied to the working electrode (vs the Ag|AgCl reference electrode), while the current was recorded.

Fluidic Assay

The modified electrode cover sheets and reagent pads were prepared as described above. A volume of 95 μL of sample was added to the inlet of the device to initiate flow and sequential delivery of reagents and the device was connected to PalmSens4. Once the blue dye visibly reached the detection channel, a 0.0 V potential was applied and current was measured until the peak was complete.

Electrochemical Data Processing

For the data collected using the static detection method, the current from the chronoamperograms was averaged over 10 s centered at 60 s for three or six measurements. For fluidic experiments, the highest point of the current peak from the amperogram was averaged for each device for three devices.

RESULTS AND DISCUSSION

Electrochemical Capillary Driven Immunoassay Device and Mechanism

SARS-CoV-2 virus contains multiple structural proteins that can be used as the target for diagnostic assays including the envelope spike glycoprotein (S protein), envelope protein (E protein), membrane protein (M protein), helicase (Hel), and nucleocapsid protein (N protein).[44] Other works have also detected SARS-CoV-2 RNA as the target.[45] Early in the SARS-CoV-2 diagnostic development literature (and still now), S protein was a popular target choice.[46−53] S protein detection received considerable attention because it is responsible for the coronavirus iconic structure, plays a vital role in infection of host cells, and induces an immune response.[54] The N protein and the S protein in SARS-CoV-2 both produce specific antibody responses,[55] and these are both now commercially available for purchase. For this work, N protein was chosen as the analyte. In SARS-CoV-2 virus particles, the ratio in number of N:S proteins was found to be 1000:100, respectively,[56] which could lead to better sensitivity with more detectable analyte per virus. Other antibody-based assays that have been made for both SARS-CoV-2 S and N proteins have shown a lower LOD for N protein vs S protein.[57]

This work introduces a device that automates the steps of a sandwich ELISA with an electrochemical detection and only requires one final user step. The presented electrochemical capillary driven immunoassay (eCaDI) device consists of alternating layers of polyethylene terephthalate (PET) and double-sided adhesive (DSA) as shown in Figure 1A. The flow channels are cut and assembled entirely in a CO_2 laser cutter which eliminates some of the difficulty of aligning layers that has been previously reported for similar device.[26,28,29] The assembly in the laser cutter was achieved by optimizing laser parameters to only cut through intended layers at a time in different steps so that the different channels could be created without outside assembly even with varying channel heights. The fluidic channels were sealed by the electrode cover sheet cut from PET with a screen-printed carbon electrode. Similar screen-printed electrodes have frequently been used for biosensing applications due to their low-cost and well-studied characteristics.[58−61] Cyclic voltammograms of a redox probe measured with 24 different electrodes can be found in Figure SI2, demonstrating their electrochemical behavior and reproducibility. The middle three layers (DSA/PET/DSA) define a channel height of 200 μm for all the channels except the channel that flows over the electrode which has a height of 50 μm. The reagent pads contain dried HRP-labeled antibody (yellow pad) and the TMB substrate (blue pad). The sample inlet has a half moon (shown in Figure 1A on the third and fourth layer from the top) with the 50 μm height which forces the sample to flow through the detection channel first before filling other channels.

Figure 1B illustrates the function of the device for sample and reagent delivery demonstrated with dyes, and Figure 1C summarizes the sensing mechanism of the eCaDI. A video of the device running can also be found in the SI. Briefly, the electrode is modified by drying the anti-N protein capture antibody and aged casein blocker, binding through passive adsorption. After the device is fully assembled, the sample is added to the inlet and the sample flows over the modified electrode (Figure 1B,i). Flow is induced by the passive pump waste pad and the PET sheets forming the bottom of the channels have a hydrophilic coating that encourages the continuous movement of the sample through the device. If present in the sample, the N protein is captured by the antibody on the electrode surface. Simultaneously, the remaining channels fill and rehydrate the reagent storage pads. Due to the difference in channel lengths the HRP-labeled anti-N protein antibody is hydrated and delivered first and, if the N protein is present, will bind to it (Figure 1B,ii). Finally, the TMB is delivered to the electrode and the measurement is recorded (Figure 1B,iii).

Reagent delivery was simulated using dyes added to reagent pads in addition to the reagents in all devices used for this study. The HRP-labeled antibody was delivered to the electrode on average at 4:17 ± 0:50 following sample addition, and the TMB was delivered at 14:45 ± 1:26 (n = 46) (Table SI2). The total measurement (started as the TMB is delivered) reported in this work can take 6−12 min; however, since the peak height is used to determine the presence of virus, in its final application the measurement would be able to stop as soon as the current begins decreasing. Overall, compared to traditional ELISAs, eCaDI greatly reduces the time required for a full sandwich immunoassay. After the sample is added, the eCaDI assay is typically completed in under 25 min with one user step, whereas a full traditional sandwich ELISA or rt-PCR test can require 5+ h with many steps that require trained personnel.

Evaluation of Electrode Modification for SARS-CoV-2 Detection

Before integrating the electrodes into the eCaDI, the electrode modification was studied independently. Our group previously reported a method in which the capture antibody and aged casein were incubated for 1 h each and required manual washing steps between incubations.[62] Initially, the same

https://doi.org/10.1021/acsmeasuresciau.2c00037
ACS Meas. Sci. Au 2022, 2, 584−594

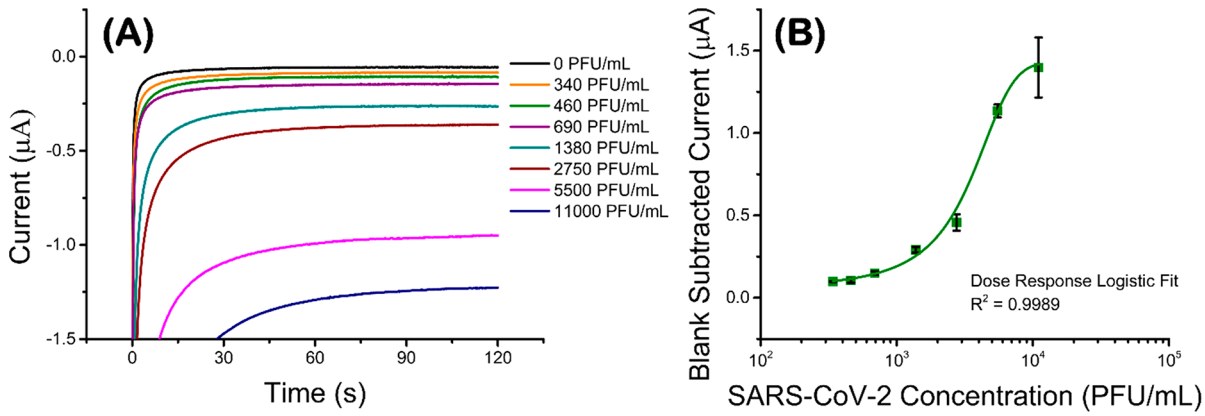

Figure 2. (A) Representative chronoamperograms for varying concentrations of inactivated SARS-CoV-2 virus in SPB taken on modified electrodes outside of the eCaDI using the static electrochemical detection method. Potential held at 0.0 V vs AglAgCl reference for 2 min. (B) Corresponding calibration curve plotted on a log scale showing blank subtracted current. Symbols and error bars represent average and standard deviation over a 10 s interval centered on 60 s (n = 3). Data is fit with a dose−response logistic fit.

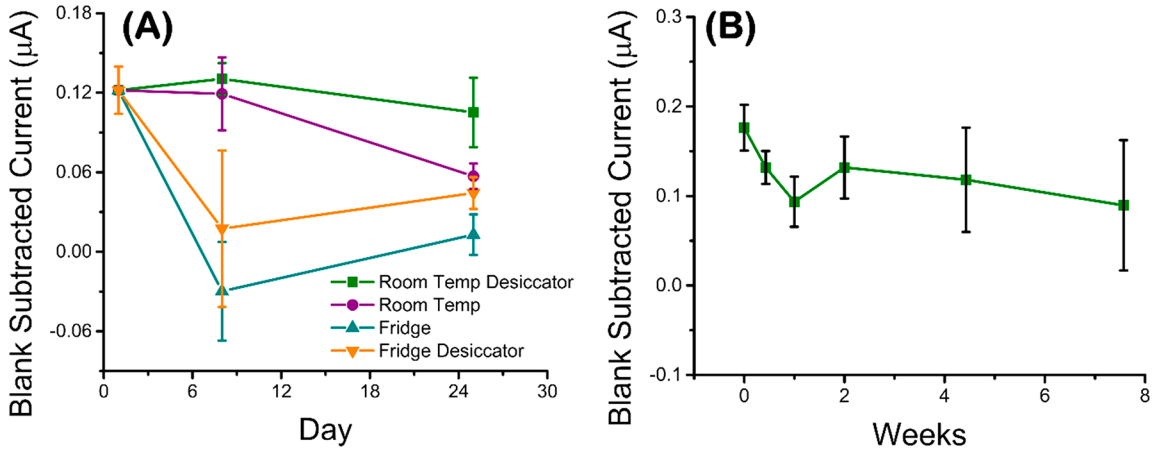

Figure 3. (A) Plot showing stability of blank subtracted current for modified electrodes in different storage conditions. Data is from chronoamperometry recorded using the static electrochemical detection method for 1380 equiv PFU/mL inactivated SARS-CoV-2 minus the blank current. Mean and error are from three electrodes ran for each day and for each condition. (B) Plot showing stability of blank subtracted current for modified electrodes stored in a desiccator at room temperature. Data is from chronoamperometry recorded static electrochemical detection method for equivalent 1380 equiv PFU/mL inactivated SARS-CoV-2 in SPB minus the blank current with SPB. Symbols and error bars represent average and standard deviation over a 10 s interval centered on 60 s (n = 8).

incubation and washing steps were used to modify the electrode before incorporation into the device. While there were significant signal differences between the blank and SARS-CoV-2 (representative amperograms shown in Figure SI3), these steps were not practical for the long-term goals of the device. The previous modification required 1.75 h. Here, the capture antibody is dried completely in a 37 °C incubator, which typically takes 30−40 min. The aged casein is then dried on the working electrode in ambient conditions, typically dried in under 15 min, bringing the total modification time to under 1 h. The aged casein blocks the surface of the electrode where there is no capture antibody to prevent nonspecific adsorption of interferents and the HRP-labeled antibodies. In addition to greatly reducing the time required to under 1 h for both modification steps, this method eliminates the need for manual washing steps and significantly less antibody and reagents are needed making this method more cost-effective for manufacturing. The washing steps also negatively altered the hydrophilicity of the PET films used for the devices which impeded flow. Figure 2A shows the current responses for varying concentrations of SARS-CoV-2 inactivated virus. Although the assay is specifically detecting N protein, concentrations are reported in equivalent plaque forming units (PFU)/mL which only quantifies viral particles capable of infection. This unit was chosen because the end goal of this device is to detect active infection and the limited quantification techniques capable of being performed in a BSL-3 cabinet. Stock virus solutions were titered to get these values, and more information can be found in Methods. A clear difference can be seen in the current response for each concentration, and the resulting calibration curve (Figure 2B) demonstrates the concentration dependent signal for concentrations ranging from 340 to 11 000 equiv PFU/mL. The data are fit to a dose−response logistic fit and present a sigmoidal shape, which is expected for immunoassays.[63,64] The LOD for this assay was calculated to be 68 equiv PFU/mL using the theoretical blank plus 3 times the standard deviation of the blank. More details on the fit and calculation can be found in the SI. This calculated LOD is comparable to or lower than the measured LOD of most commercially available rapid antigen tests, which are typically between 80 and 500 equiv PFU/mL.[65,66] Many of these LODs, however, were measured and

https://doi.org/10.1021/acsmeasuresciau.2c00037
ACS Meas. Sci. Au 2022, 2, 584−594

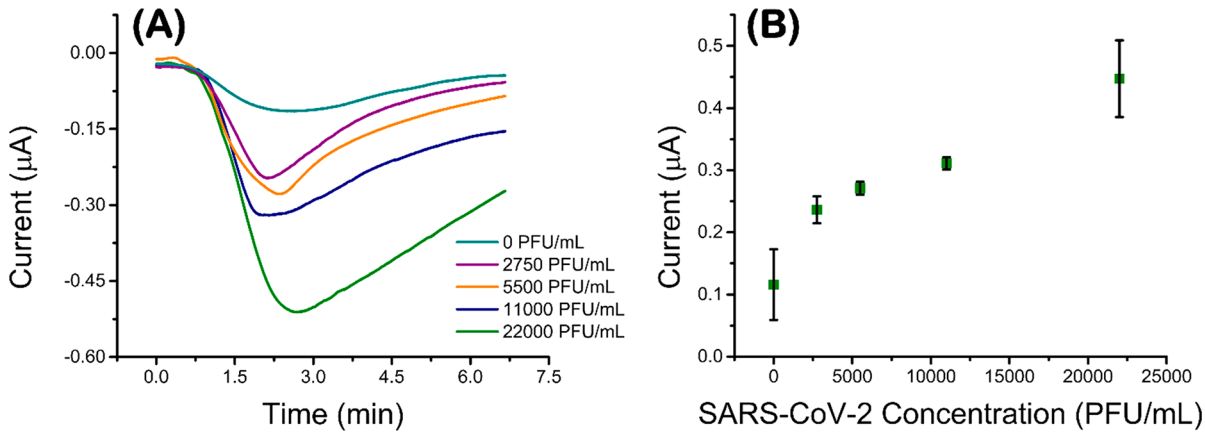

Figure 4. (A) Representative amperograms from full eCaDI device for varying concentration of SARS-CoV-2 in SPB (n = 3). Potential was held at 0.0 V for the duration of the runs. Data was time-aligned with TMB delivery to the electrode. (B) Corresponding plot of various concentrations of inactivated SARS-CoV-2 virus in SPB. Symbols and error bars represent average and standard deviation of peak current from amperograms (n = 3 for each blank and concentration).

not calculated LODs. The lowest concentration tested by the modified SARS-CoV-2 electrodes reported here was 340 equiv PFU/mL. Long-term future work should determine the LOD by serial dilution measurements to have a more realistic understanding of the sensors' capabilities at low concentrations. While the drying process as opposed to incubation may have resulted in a slight loss of signal compared to the method our group reported before,[62] this method is much more practical heading toward manufacturing and its working range and LOD are still sufficient for most COVID-19 cases, which have an extremely wide range of concentration from 5 to 10^6 equivalent PFU/mL.[67] Higher infectivity has also been shown to be correlated with higher equivalent PFU/mL values.[68]

Stability of Electrode Modification

To determine the ideal storage conditions for the electrodes after modification, four conditions were tested: with and without desiccant, at 5 °C and at room temperature. These conditions were chosen because they would be easily implemented in a commercial setting. The plot showing the stability over 24 days for each condition can be found in Figure 3A. The electrode signal was most stable at room temperature with desiccant. The other storage conditions resulted in a decrease in signal likely from loss of antibody activity of the modification over time. Many other sensors with immobilized antibodies have been found to store better in dry conditions, due to faster protein degradation in humid environments.[69−71] It is interesting that ambient temperature resulted in better signal because the majority of literature reports for various storage temperatures have shown that 4−5 °C is optimal storage for antibody based sensors.[69,72] Several theories to explain this could be increased humidity in the fridge even in a desiccator or perhaps the electrochemical signal of the SPCE (as opposed to the modification itself) is impacted by the lower temperature. The exact mechanism still remains unclear and was outside the scope of the current investigation.

After the storage conditions with desiccant at room temperature were chosen, a long-term stability study was performed, and the results are shown in Figure 3B. After an initial decrease in the first several days, the electrode response remained stable between 0.09 and 0.13 μA for 1380 PFU/mL inactivated SARS-CoV-2 and all within error of the other points for over 7 weeks. This stability is comparable to or better than most other reports.[72] Additionally, more controlled fabrication and storage environments would likely increase the stability and reduce the variability of the electrodes. Error in this study can stem from variability in fresh solutions made for each time point, differences in electrode fabrication and modification, as well as effects of modification stability. The long-term stability of the electrodes is promising for further real-world applications that require stability for manufacturing, shipping, and use.

Detection of Varying SARS-CoV-2 Concentrations with eCaDI Device

The full eCaDI device was used for in-flow detection of five SARS-CoV-2 concentrations. Each sample was diluted in SPB, which contains surfactant that will lyse the virus to release the N protein into the solution, and H_2O_2 that is necessary for the enzymatic reaction between the HRP and TMB substrate. Figure 4A shows representative (n = 3) amperograms of each concentration tested in the eCaDI. An increase in the cathodic current that forms a peak can be seen as the TMB flows over the electrode. With increasing viral concentration, the resulting peak current increases, demonstrating that the eCaDI produces concentration dependent signal. While amperogram peak shape varied, the peak currents were consistent within replicates. Plots of the average peak currents for each concentration are shown in Figure 4B. Additionally, this confirms that the reagents are being delivered in the appropriate sequence to perform a sandwich immunoassay and aligns with the dye delivery shown in Figure 1B. It is important to note that the blank measurement without virus present also has a current peak. The peak is likely a result of autoxidation of the TMB combined with nonspecific adsorption of the HRP-antibody to the fluidic channels and electrode. Because of the nonzero blank signal, data moving forward are blank-subtracted. Long-term, a positive diagnosis would be based on a current exceeding a target threshold. There are also noticeable differences in the shape of each amperogram, particularly later in the measurement, which can be attributed to slight differences in flow. Ideally, these differences are expected to decrease if the devices are no longer made, modified, and assembled by hand. The five concentration points presented demonstrate a general trend across a

https://doi.org/10.1021/acsmeasuresciau.2c00037
ACS Meas. Sci. Au 2022, 2, 584−594

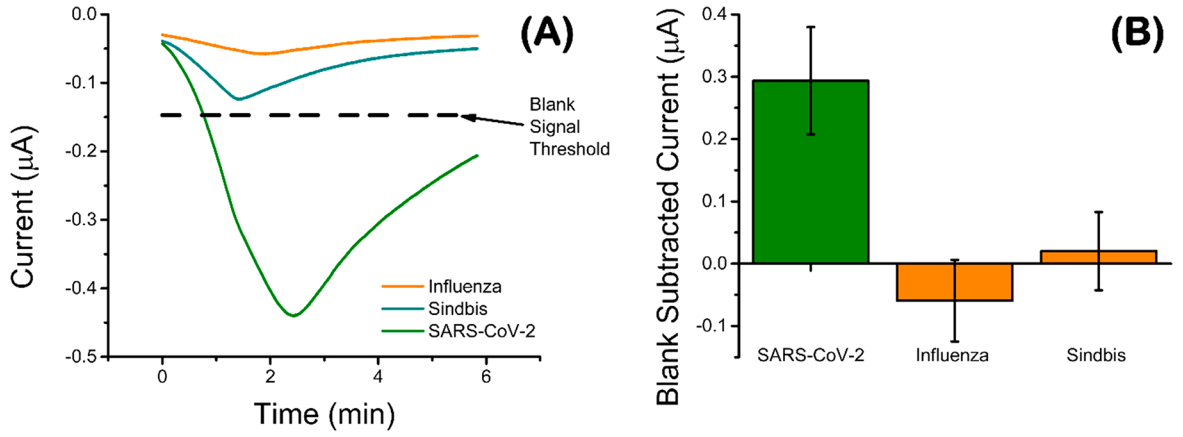

Figure 5. (A) Representative amperograms from full eCaDI device of potential interferents all at equivalent 11 000 PFU/mL (Influenza A and Sindbis) (n = 3). The black dashed line represents the average peak current of blank SPB without virus (n = 3). Potential was held at 0.0 V vs Ag|AgCl reference for the duration of the runs. Data was time-aligned with TMB delivery to the electrode. (B) Bar graph showing the blank subtracted current responses of the full eCaDI for interferents (orange) compared to the signal of SARS-CoV-2 virus (green) in SPB. Columns and error bars represent average and standard deviation of peak current from amperograms held at 0.0 V (n = 3 for each blank and interferent).

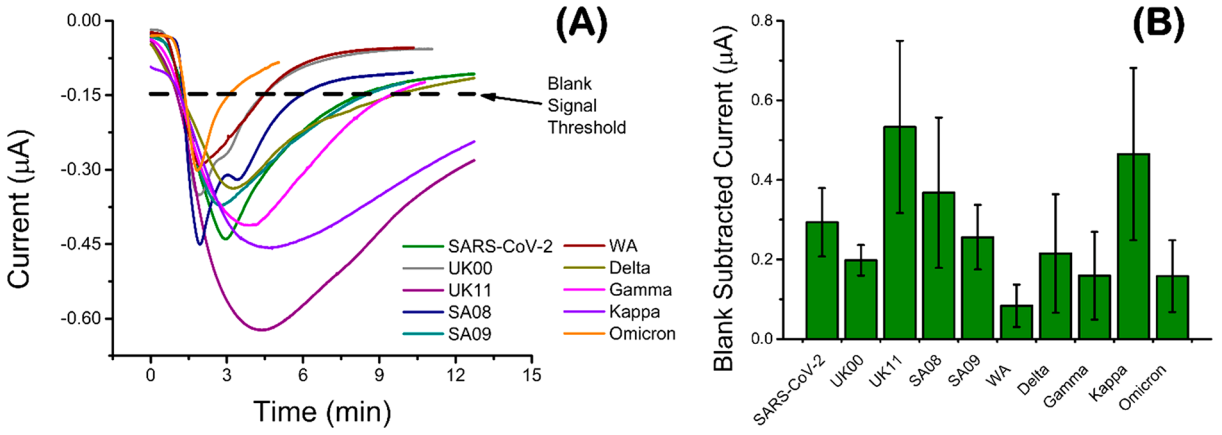

Figure 6. (A) Representative amperograms (n = 3) from full eCaDI device of variants of SARS-CoV-2 virus. The black dashed line represents the average peak current of blank SPB without virus (n = 3). Potential was held at 0.0 V vs Ag|AgCl reference for the duration of the runs. Data was time-aligned with TMB delivery to the electrode. (B) Bar graph showing the blank subtracted current responses of the full eCaDI for variants of SARS-CoV-2 virus in SPB. Columns and error bars represent average and standard deviation of peak current from amperograms held at 0.0 V (n = 3 for each blank and variant).

wide range of concentrations, and future work will continue to optimize the sensitivity of the eCaDI. There has been much discussion of sacrificing the accuracy and sensitivity of a test to improve accessibility, affordability, and timeliness of results in order to better control the spread of infectious diseases, particularly COVID-19.[73] While some sensitivity compared to a traditional sandwich ELISA is likely lost, the eCaDI meets the latter needs to address the COVID-19 pandemic as well as endemic diseases in the future.

Investigation of Potential Interferents and Ability to Detect SARS-CoV-2 Variants

To be effective, a diagnostic tool must be able to differentiate between the target, in this case SARS-CoV-2, and other viruses. To verify selectivity, the eCaDI was tested with influenza A and Sindbis virus. This is especially important for influenza A, as it presents symptoms that can easily be mistaken for COVID-19 and is a common respiratory pathogen.[74] Both interferents tested approximately at or below the signal of the average blank signal (SPB). Representative amperograms are shown in Figure 5A, and a bar graph comparing the interferent signals to that of SARS-CoV-2 is shown in Figure 5B. The negative blank-subtracted current might be due to proteins in the interferent samples blocking access of the HRP-antibodies to the electrode surface, decreasing the electron turnover by TMB. The selectivity of the eCaDI for SARS-CoV-2 demonstrates feasibility for application as a COVID-19 diagnostic.

Nine SARS-CoV-2 variants with different gene mutations were tested with the eCaDI, including UK (UK00, UK11), South African (SA08, SA09), Washington (WA), Delta, Kappa, Gamma, and Omicron. All nine variants produced positive signals above the average blank threshold, which was determined from the average of three peak currents of SPB without virus (Figure 6A). The positive results for the Omicron variant were especially encouraging, since it has significant mutations to both S and N proteins and has presented a challenge to rapid antigen tests on the market.[75] While all the variants were diluted to the same equivalent PFU/mL concentration before being tested, the signal responses varied significantly for each, which can be seen more clearly in Figure 6B. The variation is likely due to genomic differences in each that result in different N protein

https://doi.org/10.1021/acsmeasuresciau.2c00037
ACS Meas. Sci. Au 2022, 2, 584−594

expression or number of N protein per virus particle.[76] Additionally, equivalent PFU/mL, as previously mentioned, only quantifies infective virus particles not free N protein or inactive virus particles which can lead to greater variability when testing different samples as these would still be quantified in this assay.

CONCLUSION

This work presents an electrochemical capillary driven immunoassay (eCaDI) device that automates the steps of a sandwich ELISA using electrochemical detection. A drying modification technique is reported that achieves a limit of detection of 68 equiv PFU/mL. The new device greatly reduces the time required for traditional ELISA and eliminates all steps that would require trained personnel. The electrochemical detection method offers the potential for more sensitive and quantitative detection of SARS-CoV-2. The modification and device assembly methods are also promising steps toward manufacturing of similar devices. While a reasonably low limit of detection was achieved in this study, the device could be improved by further optimization of the attachment chemistry of the capture antibody to the electrode surface, the pretreatment method for the reagent pads, and the extraction buffer composition in the device. Future work will focus on detection of SARS-CoV-2 N-protein in physiological samples such as nasal swabs, improving the stability of the entire device, decreasing the time to readout, and testing compatibility with near field communication (NFC) readout. Overall, this work presents an important step to enable large scale manufacturing and commercialization of point-of-care devices for various biological analytes that have been traditionally detected using ELISA.

ASSOCIATED CONTENT

Supporting Information

The Supporting Information is available free of charge at https://pubs.acs.org/doi/10.1021/acsmeasuresciau.2c00037.

Plot of representative absorbance data for varying path lengths collected with SoloVPE to quantify antibody concentration after spun through a desalting column; table of representative plot details of absorbance data for varying path lengths collected with SoloVPE to quantify antibody concentration after spun through a desalting column used for the software to calculate the concentrations; reagent delivery times estimated by adding dyes to the reagent pads while eCaDI devices ran; CVs of screen-printed carbon electrodes; detection of SARS-CoV-2 N protein from viral samples with eCaDI (PDF)

Video of eCaDI device reagent delivery with dyes at 64× speed (MP4)

AUTHOR INFORMATION

Corresponding Author

Charles S. Henry − *Department of Chemistry and School of Biomedical Engineering, Colorado State University, Fort Collins, Colorado 80523, United States; Department of Chemical and Biological Engineering, Colorado State University, Fort Collins, Colorado 80523, United States;* orcid.org/0000-0002-8671-7728; Email: chuck.henry@colostate.edu

Authors

Kaylee M. Clark − *Department of Chemistry, Colorado State University, Fort Collins, Colorado 80523, United States*

Melissa S. Schenkel − *Department of Chemistry, Colorado State University, Fort Collins, Colorado 80523, United States*

Trey W. Pittman − *Department of Chemistry, Colorado State University, Fort Collins, Colorado 80523, United States*

Isabelle C. Samper − *Department of Chemistry, Colorado State University, Fort Collins, Colorado 80523, United States; Department of Chemical and Biological Engineering, Colorado State University, Fort Collins, Colorado 80523, United States*

Loran B. R. Anderson − *Department of Microbiology, Immunology, and Pathology, Colorado State University, Fort Collins, Colorado 80523, United States*

Wisarut Khamcharoen − *Department of Chemistry, Faculty of Science, Srinakharinwirot University, Bangkok 10110, Thailand*

Suad Elmegerhi − *Department of Microbiology, Immunology, and Pathology, Colorado State University, Fort Collins, Colorado 80523, United States*

Rushika Perera − *Department of Microbiology, Immunology, and Pathology, Colorado State University, Fort Collins, Colorado 80523, United States;* orcid.org/0000-0001-6798-2537

Weena Siangproh − *Department of Chemistry, Faculty of Science, Srinakharinwirot University, Bangkok 10110, Thailand*

Alan J. Kennan − *Department of Chemistry, Colorado State University, Fort Collins, Colorado 80523, United States*

Brian J. Geiss − *Department of Microbiology, Immunology, and Pathology and School of Biomedical Engineering, Colorado State University, Fort Collins, Colorado 80523, United States*

David S. Dandy − *Department of Chemical and Biological Engineering, Colorado State University, Fort Collins, Colorado 80523, United States; School of Biomedical Engineering, Colorado State University, Fort Collins, Colorado 80523, United States*

Complete contact information is available at: https://pubs.acs.org/10.1021/acsmeasuresciau.2c00037

Author Contributions

†K.M.C. and M.S.S. contributed equally. All authors have given approval to the final version of the manuscript. CRediT: **Melissa S. Schenkel** conceptualization (supporting), investigation (equal), methodology (equal), writing-original draft (equal), writing-review & editing (supporting); **Trey W Pittman** investigation (supporting), methodology (supporting), writing-review & editing (supporting); **Isabelle C Samper** conceptualization (supporting), investigation (equal), methodology (supporting), writing-original draft (supporting), writing-review & editing (supporting); **Loran BR Anderson** resources (equal); **Wisarut Khamcharoen** investigation (supporting), writing-review & editing (supporting); **Suad Elmegerhi** resources (supporting); **Weena Siangproh** funding acquisition (supporting), supervision (supporting), writing-review & editing (supporting); **Alan J Kennan** supervision (supporting), writing-review & editing (supporting); **Brian J. Geiss** conceptualization (equal), funding acquisition (equal), supervision (equal), writing-review & editing (equal); **David S. Dandy** resources

(supporting); **Charles S. Henry** conceptualization (equal), funding acquisition (equal), project administration (lead), supervision (lead), writing-original draft (supporting), writing-review & editing (equal).

Funding

This work was funded by the National Institutes of Health on Grant No. R01EB031510.

Notes

The authors declare no competing financial interest.

REFERENCES

(1) Ji, T.; Liu, Z.; Wang, G.; Guo, X.; Lai, C.; Chen, H.; Huang, S.; Xia, S.; Chen, B.; Jia, H.; et al. Detection of COVID-19: A review of the current literature and future perspectives. *Biosens. Bioelectron.* **2020**, *166*, 112455.

(2) U.S. Food and Drug Administration. *COVID-19 Test Basics*. https://www.fda.gov/consumers/consumer-updates/covid-19-test-basics (accessed 2022-05-23).

(3) Giri, B.; Pandey, S.; Shrestha, R.; Pokharel, K.; Ligler, F. S.; Neupane, B. B. Review of analytical performance of COVID-19 detection methods. *Anal. Bioanal. Chem.* **2021**, *413* (1), 35−48.

(4) Rai, P.; Kumar, B. K.; Deekshit, V. K.; Karunasagar, I.; Karunasagar, I. Detection technologies and recent developments in the diagnosis of COVID-19 infection. *Applied microbiology and biotechnology* **2021**, *105* (2), 441−455.

(5) Song, Q.; Sun, X.; Dai, Z.; Gao, Y.; Gong, X.; Zhou, B.; Wu, J.; Wen, W. Point-of-care testing detection methods for COVID-19. *Lab Chip* **2021**, *21* (9), 1634−1660.

(6) van Kasteren, P. B.; van Der Veer, B.; van den Brink, S.; Wijsman, L.; de Jonge, J.; van den Brandt, A.; Molenkamp, R.; Reusken, C. B.; Meijer, A. Comparison of seven commercial RT-PCR diagnostic kits for COVID-19. *Journal of Clinical Virology* **2020**, *128*, 104412.

(7) Weissleder, R.; Lee, H.; Ko, J.; Pittet, M. J. COVID-19 diagnostics in context. *Science Transl. Med.* **2020**, *12* (546), No. eabc1931.

(8) Carter, L. J.; Garner, L. V.; Smoot, J. W.; Li, Y.; Zhou, Q.; Saveson, C. J.; Sasso, J. M.; Gregg, A. C.; Soares, D. J.; Beskid, T. R.; et al. Assay techniques and test development for COVID-19 diagnosis. *ACS Cent. Sci.* **2020**, *6* (5), 591−605.

(9) Chau, C. H.; Strope, J. D.; Figg, W. D. COVID-19 clinical diagnostics and testing technology. *Pharmacotherapy: The Journal of Human Pharmacology and Drug Therapy* **2020**, *40* (8), 857−868.

(10) Mahmoudinobar, F.; Britton, D.; Montclare, J. K. Protein-based lateral flow assays for COVID-19 detection. *Protein Eng., Des. Sel.* **2021**, *34*, gzab010.

(11) Ong, D. S.; De Man, S.; Lindeboom, F. A.; Koeleman, J. G. Comparison of diagnostic accuracies of rapid serological tests and ELISA to molecular diagnostics in patients with suspected coronavirus disease 2019 presenting to the hospital. *Clin. Microbiol. Infect.* **2020**, *26* (8), 1094.e7.

(12) Basiri, A.; Heidari, A.; Nadi, M. F.; Fallahy, M. T. P.; Nezamabadi, S. S.; Sedighi, M.; Saghazadeh, A.; Rezaei, N. Microfluidic devices for detection of RNA viruses. *Reviews in medical virology* **2021**, *31* (1), 1−11.

(13) Yeo, L. Y.; Chang, H. C.; Chan, P. P.; Friend, J. R. Microfluidic devices for bioapplications. *small* **2011**, *7* (1), 12−48.

(14) Jeong, S.-G.; Kim, J.; Jin, S. H.; Park, K.-S.; Lee, C.-S. Flow control in paper-based microfluidic device for automatic multistep assays: A focused minireview. *Korean Journal of Chemical Engineering* **2016**, *33* (10), 2761−2770.

(15) Lutz, B.; Liang, T.; Fu, E.; Ramachandran, S.; Kauffman, P.; Yager, P. Dissolvable fluidic time delays for programming multi-step assays in instrument-free paper diagnostics. *Lab Chip* **2013**, *13* (14), 2840−2847.

(16) Chen, H.; Cogswell, J.; Anagnostopoulos, C.; Faghri, M. A fluidic diode, valves, and a sequential-loading circuit fabricated on layered paper. *Lab Chip* **2012**, *12* (16), 2909−2913.

(17) Giokas, D. L.; Tsogas, G. Z.; Vlessidis, A. G. Programming fluid transport in paper-based microfluidic devices using razor-crafted open channels. *Analytical chemistry* **2014**, *86* (13), 6202−6207.

(18) He, P.; Katis, I.; Eason, R.; Sones, C. Engineering fluidic delays in paper-based devices using laser direct-writing. *Lab Chip* **2015**, *15* (20), 4054−4061.

(19) Lai, Y.-T.; Tsai, J.-S.; Hsu, J.-C.; Lu, Y.-W. Automated paper-based devices by microfluidic timing-valve for competitive ELISA. In *2017 IEEE 30th International Conference on Micro Electro Mechanical Systems (MEMS)*; IEEE: 2017; pp 1321−1324.

(20) Apilux, A.; Ukita, Y.; Chikae, M.; Chailapakul, O.; Takamura, Y. Development of automated paper-based devices for sequential multistep sandwich enzyme-linked immunosorbent assays using inkjet printing. *Lab Chip* **2013**, *13* (1), 126−135.

(21) Fu, E.; Lutz, B.; Kauffman, P.; Yager, P. Controlled reagent transport in disposable 2D paper networks. *Lab Chip* **2010**, *10* (7), 918−920.

(22) Gong, M. M.; Sinton, D. Turning the page: advancing paper-based microfluidics for broad diagnostic application. *Chem. Rev.* **2017**, *117* (12), 8447−8480.

(23) Nguyen, M. P.; Meredith, N. A.; Kelly, S. P.; Henry, C. S. Design considerations for reducing sample loss in microfluidic paper-based analytical devices. *Analytica chimica acta* **2018**, *1017*, 20−25.

(24) Yetisen, A. K.; Akram, M. S.; Lowe, C. R. Paper-based microfluidic point-of-care diagnostic devices. *Lab Chip* **2013**, *13* (12), 2210−2251.

(25) Jang, I.; Carrão, D. B.; Menger, R. F.; Moraes de Oliveira, A. R.; Henry, C. S. Pump-free microfluidic rapid mixer combined with a paper-based channel. *ACS sensors* **2020**, *5* (7), 2230−2238.

(26) Jang, I.; Kang, H.; Song, S.; Dandy, D. S.; Geiss, B. J.; Henry, C. S. Flow control in a laminate capillary-driven microfluidic device. *Analyst* **2021**, *146* (6), 1932−1939.

(27) Jang, I.; Berg, K. E.; Henry, C. S. Viscosity measurements utilizing a fast-flow microfluidic paper-based device. *Sens. Actuators, B* **2020**, *319*, 128240.

(28) Carrell, C.; Link, J.; Jang, I.; Terry, J.; Scherman, M.; Call, Z.; Panraksa, Y.; Dandy, D. S.; Geiss, B. J.; Henry, C., Point-of-Need Disposable ELISA System for COVID-19 Serology Testing. *ChemRxiv*, October 20, **2021**, ver. 3. DOI: 10.26434/chemrxiv-2021-c4bmd-v3 (accessed 2022-06-01).

(29) Samper, I. C.; Sánchez-Cano, A.; Khamcharoen, W.; Jang, I.; Siangproh, W.; Baldrich, E.; Geiss, B. J.; Dandy, D. S.; Henry, C. S. Electrochemical Capillary-Flow Immunoassay for Detecting Anti-SARS-CoV-2 Nucleocapsid Protein Antibodies at the Point of Care. *ACS sensors* **2021**, *6* (11), 4067−4075.

(30) Moreira, N. S.; Chagas, C. L.; Oliveira, K. A.; Duarte-Junior, G. F.; de Souza, F. R.; Santhiago, M.; Garcia, C. D.; Kubota, L. T.; Coltro, W. K. Fabrication of microwell plates and microfluidic devices in polyester films using a cutting printer. *Anal. Chim. Acta* **2020**, *1119*, 1−10.

(31) Morbioli, G. G.; Mazzu-Nascimento, T.; Stockton, A. M.; Carrilho, E. Technical aspects and challenges of colorimetric detection with microfluidic paper-based analytical devices (μPADs)-A review. *Analytica chimica acta* **2017**, *970*, 1−22.

(32) Kaya, H. O.; Cetin, A. E.; Azimzadeh, M.; Topkaya, S. N. Pathogen detection with electrochemical biosensors: Advantages, challenges and future perspectives. *J. Electroanal. Chem.* **2021**, *882*, 114989.

(33) Mak, W. C.; Beni, V.; Turner, A. P. Lateral-flow technology: From visual to instrumental. *TrAC Trends in Analytical Chemistry* **2016**, *79*, 297−305.

(34) Trojanowicz, M. Recent developments in electrochemical flow detections—a review: part I., Flow analysis and capillary electrophoresis. *Analytica chimica acta* **2009**, *653* (1), 36−58.

(35) Noviana, E.; McCord, C. P.; Clark, K. M.; Jang, I.; Henry, C. S. Electrochemical paper-based devices: Sensing approaches and progress toward practical applications. *Lab Chip* **2020**, *20* (1), 9−34.
(36) Singh, B.; Flampouri, E.; Dempsey, E. Electrochemical enzyme-linked immunosorbent assay (e-ELISA) for parasitic nematode Ostertagia ostertagi (brown stomach worm) infections in dairy cattle. *Analyst* **2019**, *144* (19), 5748−5754.
(37) Rossier, J. S.; Girault, H. H. Enzyme linked immunosorbent assay on a microchip with electrochemical detection. *Lab Chip* **2001**, *1* (2), 153−157.
(38) Bhimji, A.; Zaragoza, A. A.; Live, L. S.; Kelley, S. O. Electrochemical enzyme-linked immunosorbent assay featuring proximal reagent generation: detection of human immunodeficiency virus antibodies in clinical samples. *Analytical chemistry* **2013**, *85* (14), 6813−6819.
(39) Grant, B. D.; Anderson, C. E.; Williford, J. R.; Alonzo, L. F.; Glukhova, V. A.; Boyle, D. S.; Weigl, B. H.; Nichols, K. P. SARS-CoV-2 coronavirus nucleocapsid antigen-detecting half-strip lateral flow assay toward the development of point of care tests using commercially available reagents. *Analytical chemistry* **2020**, *92* (16), 11305−11309.
(40) Ramachandran, S.; Fu, E.; Lutz, B.; Yager, P. Long-term dry storage of an enzyme-based reagent system for ELISA in point-of-care devices. *Analyst* **2014**, *139* (6), 1456−1462.
(41) Case, J. B.; Bailey, A. L.; Kim, A. S.; Chen, R. E.; Diamond, M. S. Growth, detection, quantification, and inactivation of SARS-CoV-2. *Virology* **2020**, *548*, 39−48.
(42) Steel, J. J.; Henderson, B. R.; Lama, S. B.; Olson, K. E.; Geiss, B. J. Infectious alphavirus production from a simple plasmid transfection. *Virol. J.* **2011**, *8* (1), 1−8.
(43) Huprikar, J.; Rabinowitz, S. A simplified plaque assay for influenza viruses in Madin-Darby kidney (MDCK) cells. *Journal of virological methods* **1980**, *1* (2), 117−120.
(44) Kudr, J.; Michalek, P.; Ilieva, L.; Adam, V.; Zitka, O. COVID-19: A challenge for electrochemical biosensors. *TrAC Trends in Analytical Chemistry* **2021**, *136*, 116192.
(45) Crevillen, A. G.; Mayorga-Martinez, C. C.; Vaghasiya, J. V.; Pumera, M. 3D-Printed SARS-CoV-2 RNA Genosensing Microfluidic System. *Advanced materials technologies* **2022**, *7*, 2101121.
(46) Pinals, R. L.; Ledesma, F.; Yang, D.; Navarro, N.; Jeong, S.; Pak, J. E.; Kuo, L.; Chuang, Y.-C.; Cheng, Y.-W.; Sun, H.-Y.; et al. Rapid SARS-CoV-2 spike protein detection by carbon nanotube-based near-infrared nanosensors. *Nano Lett.* **2021**, *21* (5), 2272−2280.
(47) Mavrikou, S.; Moschopoulou, G.; Tsekouras, V.; Kintzios, S. Development of a portable, ultra-rapid and ultra-sensitive cell-based biosensor for the direct detection of the SARS-CoV-2 S1 spike protein antigen. *Sensors* **2020**, *20* (11), 3121.
(48) Mavrikou, S.; Tsekouras, V.; Hatziagapiou, K.; Paradeisi, F.; Bakakos, P.; Michos, A.; Koutsoukou, A.; Konstantellou, E.; Lambrou, G. I.; Koniari, E.; et al. Clinical Application of the Novel Cell-Based Biosensor for the Ultra-Rapid Detection of the SARS-CoV-2 S1 Spike Protein Antigen: A Practical Approach. *Biosensors* **2021**, *11* (7), 224.
(49) Perkmann, T.; Perkmann-Nagele, N.; Koller, T.; Mucher, P.; Radakovics, A.; Marculescu, R.; Wolzt, M.; Wagner, O. F.; Binder, C. J.; Haslacher, H. Anti-spike protein assays to determine SARS-CoV-2 antibody levels: a head-to-head comparison of five quantitative assays. *Microbiol. Spectr.* **2021**, *9* (1), e00247-21.
(50) Idili, A.; Parolo, C.; Alvarez-Diduk, R.; Merkoçi, A. Rapid and efficient detection of the SARS-CoV-2 spike protein using an electrochemical aptamer-based sensor. *ACS sensors* **2021**, *6* (8), 3093−3101.
(51) Ayankojo, A. G.; Boroznjak, R.; Reut, J.; Öpik, A.; Syritski, V. Molecularly imprinted polymer based electrochemical sensor for quantitative detection of SARS-CoV-2 spike protein. *Sens. Actuators, B* **2022**, *353*, 131160.
(52) Munoz, J.; Pumera, M. 3D-Printed COVID-19 immunosensors with electronic readout. *Chemical Engineering Journal* **2021**, *425*, 131433.
(53) Mayorga-Martinez, C. C.; Vyskočil, J.; Novotný, F.; Bednar, P.; Ruzek, D.; Alduhaishe, O.; Pumera, M. Collective behavior of magnetic microrobots through immuno-sandwich assay: On-the-fly COVID-19 sensing. *Appl. Mater. Today* **2022**, *26*, 101337.
(54) Huang, Y.; Yang, C.; Xu, X.-f.; Xu, W.; Liu, S.-w. Structural and functional properties of SARS-CoV-2 spike protein: potential antivirus drug development for COVID-19. *Acta Pharmacologica Sinica* **2020**, *41* (9), 1141−1149.
(55) Fenwick, C.; Croxatto, A.; Coste, A. T.; Pojer, F.; André, C.; Pellaton, C.; Farina, A.; Campos, J.; Hacker, D.; Lau, K.; et al. Changes in SARS-CoV-2 spike versus nucleoprotein antibody responses impact the estimates of infections in population-based seroprevalence studies. *J. Virol.* **2021**, *95* (3), e01828-20.
(56) Bar-On, Y. M.; Flamholz, A.; Phillips, R.; Milo, R. Science Forum: SARS-CoV-2 (COVID-19) by the numbers. *elife* **2020**, *9*, No. e57309.
(57) Fabiani, L.; Saroglia, M.; Galatà, G.; De Santis, R.; Fillo, S.; Luca, V.; Faggioni, G.; D'Amore, N.; Regalbuto, E.; Salvatori, P.; et al. Magnetic beads combined with carbon black-based screen-printed electrodes for COVID-19: A reliable and miniaturized electrochemical immunosensor for SARS-CoV-2 detection in saliva. *Biosens. Bioelectron.* **2021**, *171*, 112686.
(58) Singh, S.; Wang, J.; Cinti, S. An Overview on Recent Progress in Screen-Printed Electroanalytical (Bio) Sensors. *ECS Sens. Plus* **2022**, *1* (2), 023401.
(59) Taleat, Z.; Khoshroo, A.; Mazloum-Ardakani, M. Screen-printed electrodes for biosensing: a review (2008−2013). *Microchimica Acta* **2014**, *181* (9), 865−891.
(60) Beitollahi, H.; Mohammadi, S. Z.; Safaei, M.; Tajik, S. Applications of electrochemical sensors and biosensors based on modified screen-printed electrodes: a review. *Analytical Methods* **2020**, *12* (12), 1547−1560.
(61) Couto, R.; Lima, J.; Quinaz, M. Recent developments, characteristics and potential applications of screen-printed electrodes in pharmaceutical and biological analysis. *Talanta* **2016**, *146*, 801−814.
(62) Samper, I. C.; McMahon, C. J.; Schenkel, M. S.; Clark, K. M.; Khamcharoen, W.; Anderson, L. B.; Terry, J. S.; Gallichotte, E. N.; Ebel, G. D.; Geiss, B. J.; et al. Electrochemical Immunoassay for the Detection of SARS-CoV-2 Nucleocapsid Protein in Nasopharyngeal Samples. *Anal. Chem.* **2022**, *94* (11), 4712−4719.
(63) Dudley, R.; Edwards, P.; Ekins, R.; Finney, D.; McKenzie, I.; Raab, G.; Rodbard, D.; Rodgers, R. Guidelines for immunoassay data processing. *Clinical chemistry* **1985**, *31* (8), 1264−1271.
(64) Cox, K. L.; Devanarayan, V.; Kriauciunas, A.; Manetta, J.; Montrose, C.; Sittampalam, S. Immunoassay methods. In *Assay Guidance Manual*, 2019; pp 1−39.
(65) Cubas-Atienzar, A. I.; Kontogianni, K.; Edwards, T.; Wooding, D.; Buist, K.; Thompson, C. R.; Williams, C. T.; Patterson, E. I.; Hughes, G. L.; Baldwin, L.; et al. Limit of detection in different matrices of 19 commercially available rapid antigen tests for the detection of SARS-CoV-2. *Sci. Rep.* **2021**, *11* (1), 1−8.
(66) Corman, V. M.; Haage, V. C.; Bleicker, T.; Schmidt, M. L.; Mühlemann, B.; Zuchowski, M.; Jo, W. K.; Tscheak, P.; Möncke-Buchner, E.; Müller, M. A.; et al. Comparison of seven commercial SARS-CoV-2 rapid point-of-care antigen tests: a single-centre laboratory evaluation study. *Lancet Microbe* **2021**, *2* (7), e311−e319.
(67) Lin, Y.-C.; Malott, R. J.; Ward, L.; Kiplagat, L.; Pabbaraju, K.; Gill, K.; Berenger, B. M.; Hu, J.; Fonseca, K.; Noyce, R. S.; et al. Detection and quantification of infectious severe acute respiratory coronavirus-2 in diverse clinical and environmental samples. *Sci. Rep.* **2022**, *12*, 5418.
(68) Karimzadeh, S.; Bhopal, R.; Tien, H. N. Review of infective dose, routes of transmission and outcome of COVID-19 caused by the SARS-COV-2: comparison with other respiratory viruses. *Epidemiol. Infect.* **2021**, *149*, No. e96.
(69) Kaduskar, O.; Bhatt, V.; Prosperi, C.; Hayford, K.; Hasan, A. Z.; Deshpande, G. R.; Tilekar, B.; Vivian Thangaraj, J. W.; Kumar, M. S.; Gupta, N.; et al. Optimization and stability testing of four

https://doi.org/10.1021/acsmeasuresciau.2c00037
ACS Meas. Sci. Au 2022, 2, 584−594

commercially available dried blood spot devices for estimating measles and rubella IgG antibodies. *mSphere* **2021**, *6* (4), No. e00490=21.
(70) Flounders, A.; Brandon, D.; Bates, A. Patterning of immobilized antibody layers via photolithography and oxygen plasma exposure. *Biosens. Bioelectron.* **1997**, *12* (6), 447−456.
(71) Li, X.; Liu, X. A microfluidic paper-based origami nanobiosensor for label-free, ultrasensitive immunoassays. *Adv. Healthcare Mater.* **2016**, *5* (11), 1326−1335.
(72) Li, F.; You, M.; Li, S.; Hu, J.; Liu, C.; Gong, Y.; Yang, H.; Xu, F. Paper-based point-of-care immunoassays: Recent advances and emerging trends. *Biotechnology advances* **2020**, *39*, 107442.
(73) Peeling, R. W.; Olliaro, P. L.; Boeras, D. I.; Fongwen, N. Scaling up COVID-19 rapid antigen tests: promises and challenges. *Lancet infectious diseases* **2021**, *21* (9), e290−e295.
(74) Osman, M.; Klopfenstein, T.; Belfeki, N.; Gendrin, V.; Zayet, S. A comparative systematic review of COVID-19 and influenza. *Viruses* **2021**, *13* (3), 452.
(75) Osterman, A.; Badell, I.; Basara, E.; Stern, M.; Kriesel, F.; Eletreby, M.; Öztan, G. N.; Huber, M.; Autenrieth, H.; Knabe, R.; et al. Impaired detection of omicron by SARS-CoV-2 rapid antigen tests. *Med. Microbiol. Immunol.* **2022**, *211*, 105.
(76) Almubaid, Z.; Al-Mubaid, H. Analysis and comparison of genetic variants and mutations of the novel coronavirus SARS-CoV-2. *Gene reports* **2021**, *23*, 101064.

https://doi.org/10.1021/acsmeasuresciau.2c00037
ACS Meas. Sci. Au 2022, 2, 584−594